Cooperative Supramolecular Block Copolymerization for the Synthesis of Functional Axial Organic Heterostructures

Cooperative Supramolecular Block Copolymerization for the Synthesis of Functional Axial Organic Heterostructures

Aritra Sarkar,[§] Tejmani Behera,[ξ] Ranjan Sasmal,[§] Riccardo Capelli,[†] Charly Empereur-mot,[‡] Jaladhar Mahato,[ξ] Sarit S. Agasti,*[,§] Giovanni M. Pavan,*[,†,‡] Arindam Chowdhury,*[,ξ] and Subi J. George*[,§]

[§] New Chemistry Unit and School of Advanced Materials (SAMat), Jawaharlal Nehru Centre for Advanced Scientific Research (JNCASR), Jakkur, Bangalore, India-560064.

[ξ] Department of Chemistry, Indian Institute of Technology Bombay, Powai, Mumbai, 400076, India.

[†] Department of Applied Science and Technology, Politecnico di Torino, Corso Duca degli Abruzzi24, 10129 Torino, Italy.

[‡] Department of Innovative Technologies, University of Applied Sciences and Arts of Southern Switzerland, Galleria 2, Via Cantonale 2c, CH-6928 Manno, Switzerland.

ABSTRACT: Supramolecular block copolymerzation with optically or electronically complementary monomers provides an attractive bottom-up approach for the non-covalent synthesis of nascent axial organic heterostructures, which promises to deliver useful applications in energy conversion, optoelectronics, and catalysis. However, the synthesis of supramolecular block copolymers (BCPs) constitutes a significant challenge due to the exchange dynamics of non-covalently bound monomers and hence requirs a fine microstructure control. Furthermore, temporal stability of the segmented microstructure is a prerequisite to explore the applications of functional supramolecular BCPs. Herein, we report the cooperative supramolecular block copolymerization of fluorescent monomers in solution under thermodynamic control, for the synthesis of axial organic heterostructures with efficient light-harvesting property. The fluorescent nature of the core-substituted naphthalene diimide (cNDI) monomers enables a detailed spectroscopic probing during the supramolecular block copolymerization process to unravel a nucleation-growth mechanism, similar to that of chain copolymerization for covalent block copolymers. Structured Illumination Microscopy (SIM) imaging of BCP chains characterizes the segmented microstructure and also allows size distribution analysis to reveal the narrow polydispersity (polydispersity index (PDI) ~ 1.1) for the individual block segments. Spectrally-resolved fluorescence microscopy on single block copolymerized organic heterostructures shows efficient energy migration and light-harvesting across the interfaces of linearly connected segments. Molecular dynamics and metadynamics simulations provide useful mechanistic insights into the free-energy of interaction between the monomers as well as into monomer exchange mechanisms and dynamics, which have a crucial impact on determining the copolymer microstructure. Our comprehensive spectroscopic, microscopic and computational analysis provide an unambiguous structural, dynamic and functional characterization of the supramolecular BCPs. The strategy presented here is expected to pave the way for the synthesis of multi-component organic heterostructures for various functions.

Introduction

The field of supramolecular polymers have emerged as an important research topic over the last two decades for the realization of ordered, nanostructured materials with adaptive and reversible functions.[1] Synthesis of supramolecular copolymers,[2] having multiple monomeric components, with microstructural control is considered as the ensuing level of complexity to be addressed for the design of next generation functional supramolecular materials such as organic heterostructures with nanoscale axial heterojunctions or nanostructures with reconfigurable monomer sequence for efficient functional output.[3] Although several synthetic strategies are available to tailor the monomer sequence in covalent copolymers[4], the microstructure control in supramolecular copolymers has been mostly limited to alternate[5], statistical[2a,6], and periodic arrangements[7] of monomers due to the labile nature of its constituent monomers held by non-covalent interactions. On the other hand, supramolecular block copolymers (BCPs)[1b,2a,b] with segmented microstructure containing long sequences of individual monomers would be the most functional and appealing architecture and has been considered as a holy grail for supramolecular chemists due to the monomer dynamics and difficulty in characterizing such structures.[2a]

In a pioneering work, Manners and co-workers have demonstrated supramolecular BCP structures from self-assembled cylindrical micelles of kinetically inert, poly(ferrocenyldimethylsilane) (PFS)-core containing block copolymers, using a crystallization-driven self-assembly (CDSA) approach.[8] This living crystallization methodology allowed the uniform epitaxial growth on kinetically stable seeds, by the sequential addition of soluble macromolecular

monomers to construct a plethora of block copolymer architectures.[9] However, supramolecular copolymerization of low molecular weight monomers has been a significant challenge due to the fast exchange of monomers during the non-covalent synthesis and are seldom reported. In an early attempt, Aida and co-workers have demonstrated the seeded growth of hexabenzocoronene (HBC) derived amphiphilic monomers on kinetically stable stacks of electronically complementary HBC monomers to accomplish supramolecular tri-block nanostructures.[10] Similarly, Takeuchi, Sugiyasu and co-workers have achieved supramolecular BCPs via seeded growth of porphyrin monomers using a solvent-mixing protocol,[11] in a procedure analogous to the CDSA for polymeric micelles.[8,9] To introduce an additional kinetic control for the synthesis of well-defined segmented microstructures, Würthner and co-workers have demonstrated a seed-induced living supramolecular polymerization (LSP)[2b,12,13] approach for the BCP synthesis of core substituted perylenediimide monomers.[14] Well-defined triblock supramolecular polymer architectures were made under kinetic control by introducing metastable states of one of the monomer to the seeds of another. In a similar kinetically controlled approach, we have recently reported supramolecular BCPs of fluorescent cNDI[15] monomers via heterogeneous nucleation triggered seeded supramolecular polymerization.[16] Seeded LSP process under kinetic control, is analogous to the well-established living polymerization techniques[17] for the synthesis of covalent BCPs[4] and hence has the potential for better structural control if the monomer exchange dynamics can be retarded.

Another synthetic approach to realize the covalent block copolymers is via chain-growth copolymerization by modulating the reactivity ratio of the constituting monomers[2a,18], although dispersity control is compromised to a certain extent compared to the living polymerization strategies. An equivalent non-covalent synthetic method would be a cooperative or nucleation-elongation growth supramolecular copolymerization under thermodynamic conditions.[1a,19] However, thermodynamically controlled cooperative supramolecular copolymerization often resulted in statistical,[6] periodic or gradient[20] microstructures rather than the desired block organization of the monomers, due to the lack of fine-tuning in the free energy of hetero- versus homo-monomeric interactions which determines the reactivity ratio.[2a] In a unique manifestation of supramolecular block copolymerization under thermodynamic control, recently Meijer and co-workers obtained supramolecular BCPs[21] by utilizing a balanced mismatch penalty and cooperativity difference between the two triarylamine based monomers.[22] This synthetic strategy for supramolecular BCPs could result in stable segmented microstructures[2a] and hence are ideally suited for exploring various applications.

We envisage that supramolecular block-copolymerization of organic chromophoric monomers with complementary optical or electronic properties would provide an attractive bottom-up strategy for the synthesis of axial heterostructures with designed interfaces and anisotropic energy or electron transport properties potentially useful in photovoltaics, energy conversion and supramolecular electronics.[3,23] Although inorganic axial heterostructures with two dissimilar semi-conducting components are well exploited,[24] the synthesis of analogous organic heterostructures with linear heterojunctions has been a substantial challenge. In a seminal work, Aida and co-workers have shown enhanced energy transport across the linear p-n heterojunctions of HBC derived supramolecular BCPs.[10a] Although Manners and co-workers have elegantly shown an efficient exciton transport through semiconducting cores[25] and colour tunable fluorescent multi-block nanostructures,[26] in supramolecular block micelles, the transport properties through the linear heterojunctions are not yet investigated. This scenario encouraged us to explore the energy-transport properties along the axial heterostructures at the nanoscale, by the synthesis of supramolecular BCPs of π-conjugated monomers with complementary optical properties.

Herein we report the thermodynamically controlled, solution-phase synthesis of supramolecular BCPs of fluorescent cNDI donor and acceptor monomers which have optical complementarity, to facilitate the energy transfer process along the resultant organic heterostructures. Detailed spectroscopic probing unveils a nucleation-growth mechanism for this supramolecular block-copolymerization process, controlled by the unbalance in the free energy of monomer-monomer interactions (reactivity ratio) between the monomeric species. This is corroborated by coarse-grained molecular simulations, which also reveal the rather static nature of the supramolecular polymers at room temperature. Structured illumination microscopy (SIM) imaging further provides an unambiguous characterization of the segmented microstructure of these supramolecular BCPs with a narrow size distribution of the individual segments. We further demonstrate that the degree of polymerization and the block lengths in these supramolecular block structures can be altered by modulating the monomer exchange dynamics with different annealing temperatures. Finally, spectrally resolved fluorescence microscopy studies on single supramolecular BCP with donor-acceptor-donor segmented microstructure, reveal an unprecedented energy migration and light-harvesting across the nanoscale linear heterojunctions.

Results and Discussion

Molecular design and synthesis

Supramolecular block copolymerization in solution under thermodynamic control requires two structurally similar monomers with a cooperative, nucleation-elongation growth mechanism of homopolymerization.[19,21] In order to minimize the structural mismatch between the monomers, we have used cNDI derivatives as the monomers, since its HOMO-LUMO energy levels and the resultant optoelectronic properties can be modulated by the simple core-substitution with heteroatoms having varying donor strengths.[15] In the present study, we have used ethoxy (-OEt) and pentanethiol ($-SC_5H_{11}$) cNDI derivatives (Figure 1a), which would render green and red fluorescent monomers, respectively that helps to characterize the resultant supramolecular copolymer via spectroscopic probing and fluorescence microscopic visualization. Further, we envisage that the Förster Resonance Energy Transfer (FRET) between green and red monomers can

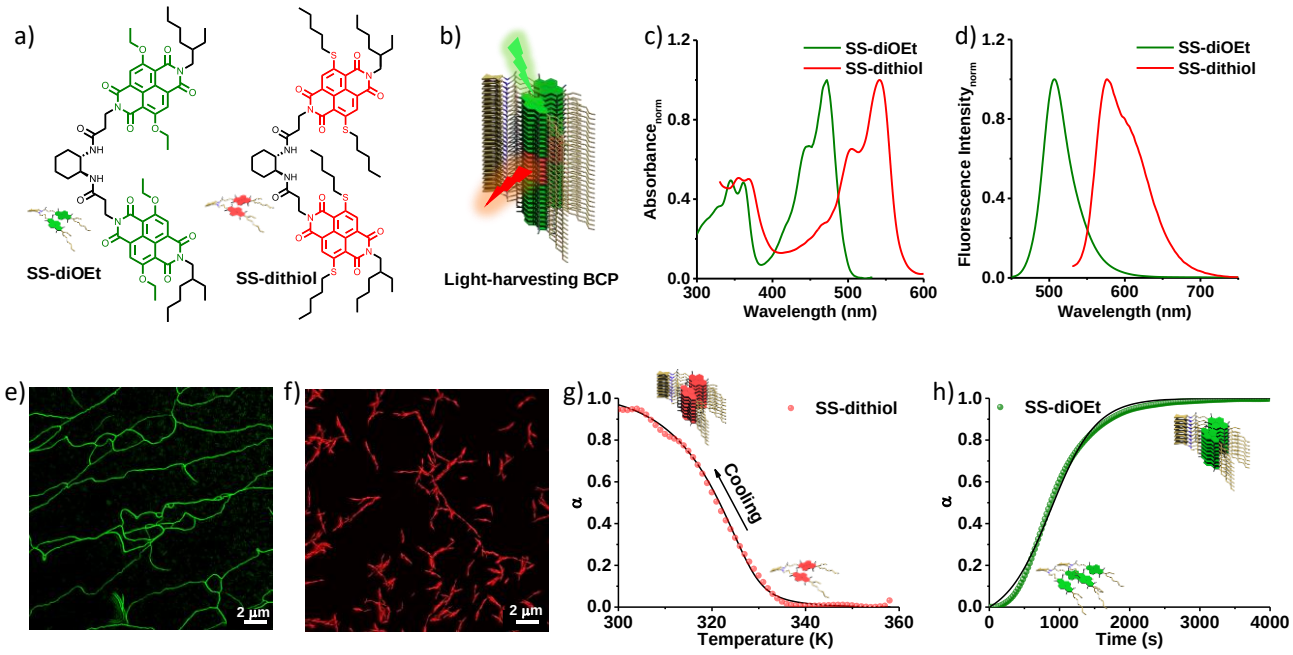

Figure 1. Molecular structures and supramolecular homopolymerization: (a) Molecular structures of **SS-diOEt** and **SS-dithiol** monomers along with its schematic. (b) Schematic representation of light-harvesting axial organic heterostructures (supramolecular BCP) with green-red-green segmented microstructure. Normalized (c) absorption and (d) emission spectra of **SS-diOEt** (λ_{ex} = 430 nm) and **SS-dithiol** (λ_{ex} = 530 nm) homopolymers showing distinct absorption and emission profiles. SIM images of (e) green (green channel) and (f) red (red channel) fluorescent 1D supramolecular homopolymers for **SS-diOEt** and **SS-dithiol**, respectively. (g) Cooling curve depicting the supramolecular homopolymerization of **SS-dithiol** monomers obtained by monitoring the CD changes at 548 nm. The non-linear curve fits well with a nucleation-elongation model (black solid line). The black arrow indicates the direction of cooling. (h) Time-dependent degree of aggregation (α) displaying the transition from the metastable state to supramolecular homopolymers of **SS-diOEt** obtained by monitoring the absorbance change at 370 nm, which could be fitted (black solid line) to an autocatalytic nucleation-elongation growth model. ([**SS-diOEt**] = [**SS-dithiol**] = 2.5×10^{-5} M, TCE/MCH, 25/75 (v/v), l = 10 mm, cooling rate is 1 K/min, (green channel: λ_{ex} = 488 nm, λ_{coll} = 495–575 nm), (red channel: λ_{ex} = 561 nm, λ_{coll} = 570–650 nm)).

be used to impart functional characteristics to resulting BCPs as light-harvesting axial organic heterostructures (Figure 1b). To facilitate a hydrogen-bonded cooperative supramolecular polymerization we have attached the cNDI π-conjugated derivatives to chiral (S,S)-trans-1,2-bis(amido)-cyclohexane motif and the resultant bischromophoric derivatives (**SS-dithiol** and **SS-diOEt**) are expected to grow by following a nucleation-elongation mechanism (Figure 1a).[27] In addition, the chiral diaminocyclohexane cores are known to induce chirality during the self-assembly to aid the chiroptical probing of the supramolecular copolymerization process.[27b]

SS-dithiol monomer was synthesized following the synthetic Schemes S1 and S2. First, a thiol group substituted cNDI derivative has been prepared by the condensation of 2-ethylhexan-1-amine, and 3-ammoniopropanoate with 1,4-dibromo substituted NDI derivative, which was followed by the substitution of core Br atoms with pentanethiol chains. Subsequent coupling of this with enantiomerically pure *trans*-1,2-bis(amido)-cyclohexane motif gave **SS-dithiol** monomer. On the other hand, **SS-diOEt** was synthesized following our earlier reports.[27b] All the molecules have been characterized by ^{1}H NMR, mass spectrometry and elemental CHNS analysis (Section A.3. in supporting information).

Mechanistic investigation of supramolecular homopolymerization

We have first investigated the mechanistic aspects of the supramolecular homopolymerization of **SS-diOEt** and **SS-dithiol** monomers. Both the monomers remain in its monomeric state in 1,1',2,2'-tetrachloroethane (TCE) solvent as evident from the sharp n-π* transition at 533 nm and π-π* transitions at 372 nm and 354 nm for **SS-dithiol** (Figure S1) and sharp n-π* transition at 472 nm along with π-π* transitions at 344 nm and 361 nm for **SS-diOEt** (Figure S5). Weak circular dichroism (CD) signal originating from the intra-chromophoric interactions and linear dependence of its g-value (anisotropy factor) on concentration, further supports the absence of intermolecular interactions in TCE for both monomers (Figure S1 and S5). Supramolecular homopolymerization of these monomers was performed in methylcyclohexane (MCH)/TCE solvent mixtures (TCE/MCH, 40/60 (v/v) to TCE/MCH, 25/75 (v/v)) and was probed by various spectroscopic changes that are very sensitive to inter-chromophoric interactions. Samples were prepared by annealing the solutions of respective monomers in appropriate solvent mixtures to 363 K followed by cooling to 298 K. Absorption spectra of **SS-dithiol** showed broadening and red-shift of the n-π* transition to 540 nm along with the reversal of vibronic intensities

of π-π* transitions at 372 nm and 354 nm with increasing percentages of MCH in TCE (TCE/MCH, 40/60 (v/v) to TCE/MCH, 25/75 (v/v), Figure S2). These changes account for the increased inter-chromophoric interactions due to hydrogen bonding promoted π-stacking of monomers. Similarly, **SS-diOEt** also exhibited a broadening of n-π* transition and reversal of vibronic intensities of π-π* transitions (Figure S5). Increased inter-chromophoric interactions on self-assembly further resulted in the appearance of a strong CD signal with maxima at 548 nm for **SS-dithiol** and 484 nm for **SS-diOEt** (Figure S2 and S5). Further investigation revealed the CD signal of **SS-diOEt** is contaminated with linear dichroism (LD).[27b] Both **SS-dithiol** and **SS-diOEt** monomers showed a bathochromic shift in emission maxima upon self-assembly, indicating a J-type slipped organization of chromophores, which is also supported by the time-resolved fluorescence decay experiments (Figure S1-S3, and S5). The green (λ_{max} = 505 nm) and red (λ_{max} = 575 nm) emission of the **SS-diOEt** and **SS-dithiol** aggregates (Figures 1c and 1d), respectively enabled its visualization through SIM, as green and red-emitting supramolecular polymers (Figures 1e, 1f, S5, and S6). Distinct absorption and emission spectral features of stacked **SS-diOEt** and **SS-dithiol** monomers facilitate the independent probing of monomers during the supramolecular copolymerization process and the orthogonal visualization using SIM microscopy. Whereas **SS-dithiol** gets excited at both green (λ_{ex} = 488 nm) and red (λ_{ex} = 561 nm), **SS-diOEt** selectively gets excited at the green, facilitating the visualization of supramolecular copolymers with different microstructure (Figure S7). On heating the homopolymers of **SS-dithiol** and **SS-diOEt** to 363 K, the CD signal decreases along with a hypsochromic shift in the absorption spectra (Figure S8 and S9), suggesting the disassembly to monomers.

To investigate the self-assembly mechanism of the supramolecular homopolymerization process, respective monomeric solutions at high temperature (363 K) were cooled slowly with a ramping rate of 1 K/min, and the degree of aggregation (α) was monitored at corresponding aggregation spectral features. The cooling curve obtained by monitoring the CD signal at 548 nm for the **SS-dithiol** monomers (c = 2.5×10^{-5} M, TCE/MCH, 25/75 (v/v)) showed a non-linear curve, which could be fitted to a nucleation-elongation model with an elongation temperature (T_e) of 323 K (Figure 1g, Table S2).[28] On the other hand, **SS-diOEt** monomers in the same solvent composition (2.5×10^{-5} M, TCE/MCH, 25/75 (v/v)) while cooling (cooling rate = 1K /min) from its monomeric solution at high temperature to 298 K gets trapped in a metastable state (Figure S11). However, the metastable state gradually gets converted into a thermodynamically stable supramolecular polymer, as evident from the time-dependent absorption changes at 370 nm. Interestingly, the obtained kinetic data could be well-fitted with an autocatalytic Watzky and Finke[29] model suggesting the presence of nucleation-elongation growth mechanism, for **SS-diOEt** monomers (Figure 1h and S11). While both **SS-dithiol** and **SS-diOEt** monomers undergo nucleation-elongation homopolymerization and forms thermodynamically stable assemblies, the **SS-diOEt** additionally provide a metastable state and a kinetic handle to control temporal aspects of the supramolecular polymerization process.

Stability and monomer exchange dynamics in supramolecular homopolymers from molecular simulations

I*n silico* investigations based on high-resolution (atomistic or fine coarse-grained) molecular models are important to complement and rationalize the experimental findings, offering a detailed insight into the structural and dynamic behavior of supramolecular polymers.[30] In particular, recently it was demonstrated that the combination of metadynamics simulations and fine coarse-grained molecular models allow to investigate the mechanisms and relative kinetics of rare monomer exchange events that occur within and in/out of the dynamic supramolecular polymers.[31] We exploited a similar approach here to explore the relative stabilities, and intrinsic dynamics of the supramolecular homopolymers of **SS-dithiol** and **SS-diOEt** studied herein. We first built all atom (AA) models for both **SS-dithiol** and **SS-diOEt** monomers (Figure 2a). We then used these as a reference to develop coarse-grained (CG) models for the same monomers (Figure 2b: resolution in the CG model is ~5 Å). As recently done for similar self-assembling monomers,[16] the CG models for the **SS-dithiol** and **SS-diOEt** monomers were developed based on the MARTINI CG force field[32] and have been further refined in order to reproduce the correct behavior of the monomers in the solvent (cyclohexane) seen in the AA models and the monomer-monomer interactions (see computational details in the Supporting Information).[30b] Using these CG models, we studied the dimerization free-energies associated with the **SS-diOEt**/**SS-diOEt**, **SS-dithiol**/**SS-diOEt**, and **SS-dithiol**/**SS-dithiol** interaction in cyclohexane (Figure 2c: green (**SS-diOEt**)-green (**SS-diOEt**), green (**SS-diOEt**)-red (**SS-dithiol**) and red (**SS-dithiol**)-red (**SS-dithiol**) dimerization ΔG values, respectively) employing Well-tempered Metadynamics (WT-MetaD)[33] simulations. The ΔG data obtained from the WT-MetaD simulations showed that the most stable interaction is the one given by **SS-diOEt** homodimer, followed by the **SS-dithiol**/**SS-diOEt** heterodimer and the **SS-dithiol** homodimer. This information is useful to understand the extent to which different monomers are likely to mix during the supramolecular copolymerization process or upon supramolecular monomer exchange in solution.

As a next step, we built two CG models of pre-formed supramolecular polymers (one for **SS-dithiol** and one for **SS-diOEt**) composed of 40 initially extended stacked monomers (Figure 2d). These CG stack models have been solvated, equilibrated, and relaxed in explicit CG cyclohexane solvent molecules by running 1 μs classical CG molecular dynamics (MD) simulations at the temperature of 300 K and pressure of 1 atm (section C.2. in supporting information). To explore the event of monomer exchange from the fibers' tips, we have performed multiple infrequent WT-MetaD simulations by activating/biasing the unbinding of the first monomer from the tip of the stacks and the release of the monomers into the cyclohexane solvent. We could observe that in both stacks the exchange event is characterized by two different steps: (1) the monomer at the stack tip closes-up in a "sandwich" conformation and (2) from such closed state, the monomer can get released to the solvent (section C.5. in supporting information).[31] We ran multiple infrequent WT-MetaD simulations

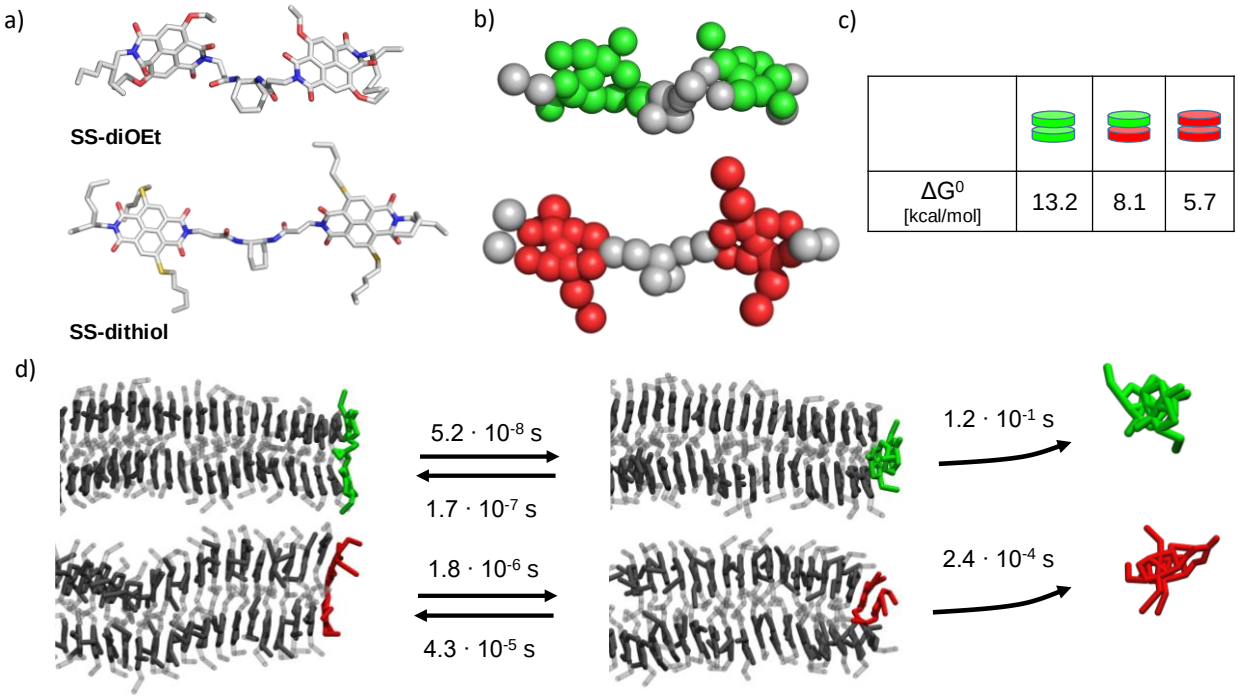

Figure 2. Molecular modeling of monomer exchange in the supramolecular polymers. (a) All-atom (AA) models of **SS-diOEt** and **SS-dithiol** (hydrogen atoms not shown for clarity) monomers. (b) Coarse-grained (CG) models for both the monomers. (c) Dimerization/binding free-energies for the **SS-diOEt**/**SS-diOEt**, **SS-diOEt**/**SS-dithiol**, and **SS-dithiol**/**SS-dithiol** interactions. (d) Schematic representation and characteristic timescales (t_{CG}) for the exchange steps involved in the process of monomer exchange from the tips in both **SS-diOEt** (top) and **SS-dithiol** (bottom) supramolecular stacks. Monomer exchange steps: (i) the monomer on the tip, starting from an open/stacked state (left), closes in "sandwich conformation" (middle), and (ii) from such closed conformation exchanges with the solution (right).

exploring step 1 (back and forth closing and opening of the tip monomer) and step 2 (exchange of a closed monomer with the solution). The transition/exchange times obtained from these WT-MetaD runs allowed us to reconstruct the unbiased kinetics for the steps involved in the monomer exchange and to estimate their characteristic timescales (Figure 2d: t_{CG}). The statistics obtained from these WT-MetaD simulations fit well with the Poissonian exchange probability distributions expected for rare exchange events, proving the appropriateness of the adopted method (see Supporting Figure S30 and section C.5. in supporting information). [31]

From these exchange distributions, we calculated the characteristic exchange timescales (*i.e.* the average residence times of the monomers on the stack tips) for the two systems (reported in Figure 2d). Although these exchange timescales are extracted from CG models and are therefore qualitative, these are nonetheless useful to compare the relative dynamics of monomer exchange from the tips of the two stacks (step 2). This event is found to be slower (less likely) in **SS-diOEt** (t_{CG} ~1.2×10^{-1} s) than in **SS-dithiol** (t_{CG}~2.4×10^{-4} s). Conversely, the closing/opening of monomers at the tip of the stacks (exchange step 1) seems to be faster in the **SS-diOEt** (closing/opening timescales, t_{close}/t_{open}, in the order of ~$10^{-8}/10^{-7}$ s) than in the **SS-dithiol** (t_{close}/t_{open} in the order of ~$10^{-6}/10^{-5}$ s). The slower dynamics and more static nature of **SS-diOEt** are in line with the higher **SS-diOEt**-**SS-diOEt** interaction energies reported in Figure 2c.

In general, in these stacks the closure into the "sandwich" conformation of the monomers at the chain-end appears to be faster than the opening, suggesting that, statistically, the tips of these stacks are intrinsically more disordered compared to the perfectly organized monomers expected in the bulk. In fact, monomers closure along the fibers introduces defects inside these stacks, while such defects are known to be important for the exchange of monomers and the overall dynamics of the assembly.[31,30b,34] A more in-depth analysis of these simulations of these fiber models indicated that at the equilibrium, both assemblies possess stacking defects at the fiber tips as well as in their interior. Analyzing the extent of solvent exposure of monomers in these stacks and the extent of ordered regions indicate that the **SS-diOEt** assembly tends to form more defects along its length with respect to the **SS- dithiol** (see Supporting Figure S31: green *vs.* red dots). This is interesting, as such defects may constitute hot spots from where the monomers can exchange in/out of the stacks[30c,31,34] and eventually leading to the mixing of monomers and assemblies during the supramolecular copolymerization process. Thus, based on this analysis the **SS-diOEt** assemblies appear overall more disordered than **SS-dithiol** ones. The relatively slow dynamics and static nature of **SS-diOEt** fibers seen in the simulations, which originates from the stronger monomer-monomer interactions in these assemblies (Figure 2c), and their higher tendency to disorder compared to **SS-dithiol** (likely leading to a lower tendency to co-monomer stacking), is in agreement with the experimental

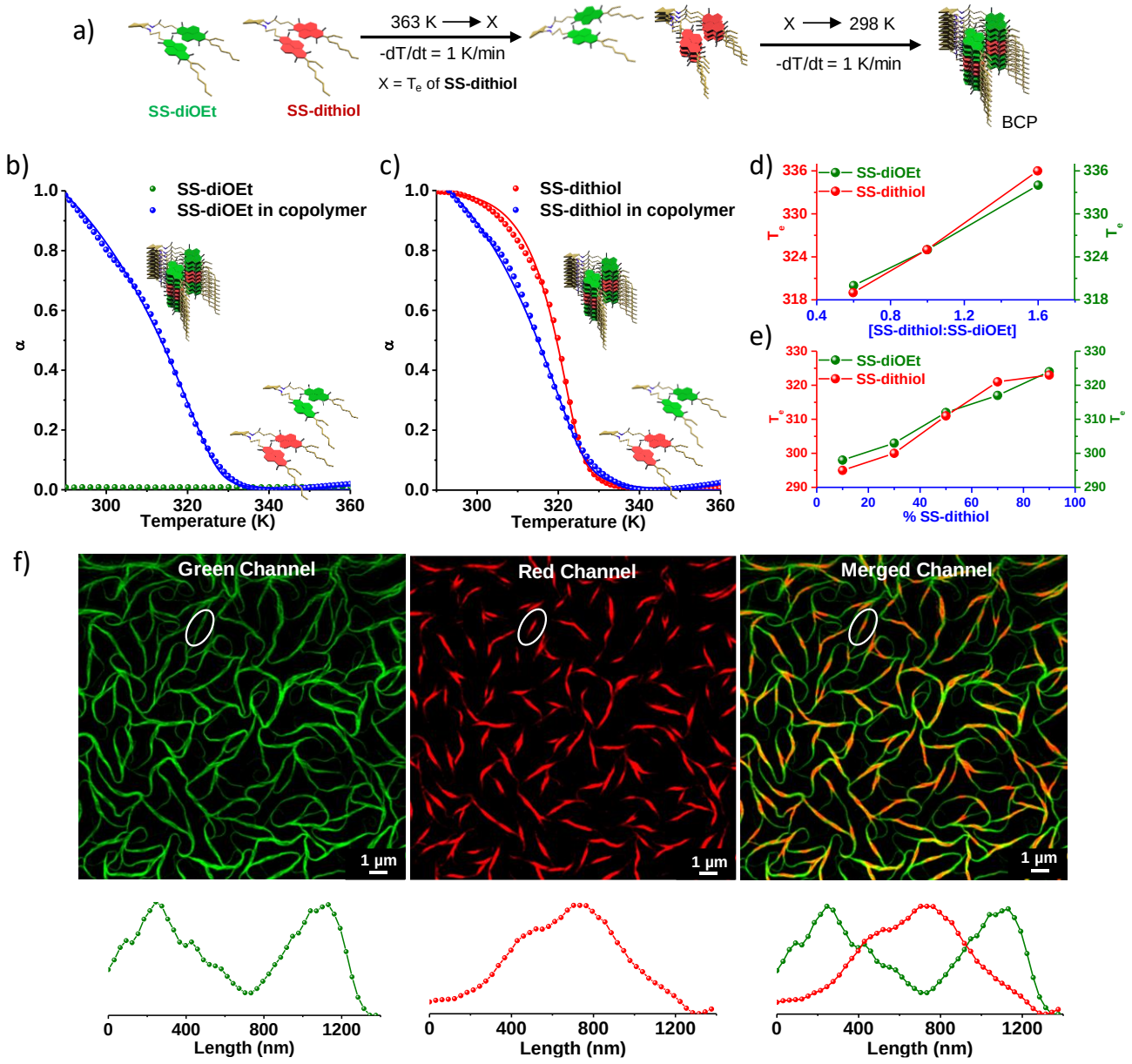

Figure 3. Cooperative Supramolecular Block Copolymerization: (a) Schematic illustration of the supramolecular block co-polymerization process, by cooling down a mixture of monomers from high temperature under thermodynamic control. Temperature-dependent degree of aggregation (1 K/min cooling rate) obtained by probing the emission changes at (b) 490 nm for **SS-diOEt** (λ_{ex} = 430 nm) and (c) 570 nm for **SS-dithiol** (λ_{ex} = 530 nm), of both homopolymers and BCP, which shows that **SS-diOEt** and **SS-dithiol** elongates at the same temperature confirming a co-assembly process. The elongation temperature (T_e) of the monomeric mixture matches well with that of pure **SS-dithiol**. (d) Plot of Te of the co-assembled solution against varying **SS-dithiol** concentration while keeping **SS-diOEt** concentration constant. (e) Plot of T_e against different **SS-dithiol:SS-diOEt** molar ratio with a fixed total concentration at 3×10^{-5} M. Green dots and red dots in figures (d) and (e) corresponds to the T_e obtained by monitoring the **SS-diOEt** and **SS-dithiol** spectral features, respectively. (f) SIM microscopy image of the co-assembled solution of **SS-diOEt** and **SS-dithiol** contains alternating green, red emitting fibers which depicts formation of supramolecular BCPs. Corresponding intensity profile of the fibers in green, red, and merged channel illustrates that the green and red emission does not overlay with each other's. The white oval shapes represent the fibers from where the intensity profiles were extracted. ([**SS-diOEt**] = [**SS-dithiol**] = 2.5×10^{-5} M, TCE/MCH, 25/75 (v/v), l = 10 mm, (green channel: λ_{ex} = 488 nm, λ_{coll} = 495–575 nm), (red channel: λ_{ex} = 561 nm, λ_{coll} = 570–650 nm)).

observation of the entrapment of **SS-diOEt** monomers into a local minimum metastable (disordered) state during its temperature-dependent supramolecular homopolymerization process. On the other hand, the faster dynamics of **SS-dithiol** assemblies may enable them to reach the thermodynamic equilibrium during the self-assembly process as seen in the experiments in a more facile way compared to **SS-diOEt**.

Supramolecular block copolymerization under thermodynamic control

Having investigated the mechanistic aspects of supramolecular homopolymerization of both **SS-dithiol** and **SS-diOEt** monomers, we next attempted the supramolecular block copolymerization process to construct the axial organic heterostructures. In general, experimentally we could observe that **SS-dithiol** forms stable supramolecular homopolymers under thermodynamic conditions while **SS-diOEt** tends fall into a kinetically trapped metastable phase prior to time-dependent supramolecular homopolymerization process. Thus, first we attempted the heterogeneous seeded supramolecular polymerization under kinetic control to construct multi-component block topology.[15] However, the introduction of **SS-dithiol** seeds into the metastable state of **SS-diOEt** does not trigger an immediate growth of later, which ruled out the possibility of heterogeneous nucleation process of the monomers under kinetic control (Figure S12). This observation was initially quite surprising. We can rationalize this considering the results from simulations. We speculate this could be due to the slower dynamics (at room temperature) of **SS-diOEt** monomers and to their higher free-energy of monomer-monomer interactions compared to that of hetero-monomeric interactions (see Figure 2c). This would make **SS-diOEt** monomers that exchange out of the **SS-diOEt** assemblies into the solution more prone to re-assemble with other **SS-diOEt** monomers (or to reassemble back onto **SS-diOEt** assemblies) rather than to stack onto **SS-dithiol** assemblies. At the same time, it is also possible that the intrinsic presence of defects at the tips of **SS-dithiol** and **SS-diOEt** stacks, originating from monomers in sandwiched conformation, might also prevent, or somehow hinder, the heterogeneous nucleation during the seeding experiments under kinetic control.

We envision that supramolecular copolymerization of the monomers under thermodynamic control[16,17], analogous to the classical chain copolymerization, would be another strategy to achieve block microstructure. Furthermore, the reactivity ratio (R) of 1.17 that can be calculated from the interaction free-energies of Figure 2c ($R = (\Delta G_{1\text{-}1}+\Delta G_{2\text{-}2})/2\times\Delta G_{1\text{-}2}$) obtained from the CG simulations suggests the possibility of generating a blocky organization during a cooperative supramolecular copolymerization similar to the chain copolymerization in covalent polymeric systems. Since **SS-dithiol** is having a red-shifted and overlapping absorption spectral features with that of the **SS-diOEt**, the growth of **SS-diOEt**, monomers cannot be selectively monitored using the absorbance changes during co-assembly process (Figure S13a). Furthermore, CD spectral features of **SS-diOEt** cannot be used to probe its growth, as it is contaminated with LD. Hence, we have utilized the distinct green (λ_{max} = 505 nm) and red (λ_{max} = 575 nm) emission of **SS-diOEt** and **SS-dithiol** monomers, respectively, which could also be selectively excited, to spectroscopically probe the growth process (Figure S13b).

In a typical supramolecular copolymerization process under thermodynamic conditions, a 1:1 mixture (c = 2.5×10^{-5} M) of **SS-diOEt** and **SS-dithiol** in 25 % TCE in MCH (v/v) solvent mixture was heated to 363 K and cooled under thermodynamic control at a rate of 1 K/min. Temperature-dependent emission changes of a 1:1 mixture of **SS-dithiol** and **SS-diOEt** obtained via selective excitation (λ_{ex} = 430 nm for **SS-diOEt** and 530 nm for **SS-dithiol**) and monitoring at 490 nm and 570 nm for **SS-dithiol** and **SS-diOEt**, respectively indicated the co-assembly between the two components. Temperature-dependent emission changes of **SS-dithiol** showed a two-step non-linear changes, which could be fitted to a cooperative nucleation-elongation model. Interestingly, the T_e of 325 K of the 1:1 monomeric mixture matches well with that of **SS-dithiol** homopolymer at the same concentration (T_e = 325 K, c = 2.5×10^{-5} M) (Figure 3c, Table S4 and S5). More importantly, the selective probing of the **SS-diOEt** emission during co-assembly, also followed a nucleation-elongation mechanism with identical T_e (325 K) as that of **SS-dithiol**, despite the fact that **SS-diOEt** homopolymer at same concentration get trapped into a metastable state under similar conditions. This provides a clear indication of heterogeneous nucleation and supramolecular copolymerization process of **SS-dithiol** and **SS-diOEt** monomers (Figure 3b, Table S4 and S5). Supramolecular copolymerization of **SS-diOEt** and **SS-dithiol** mixtures with constant **SS-diOEt** (c = 2.5×10^{-5} M) and varying **SS-dithiol** (1.5×10^{-5} to 4×10^{-5} M) concentrations, showed a decrease in T_e of the supramolecular copolymer with a decrease in **SS-dithiol** concentration (Figure 3d, S14a and S14b). Further, on the variation of monomer ratio (**SS-dithiol:SS-diOEt** from 9:1 to 1:9) by keeping the total concentration constant (3×10^{-5} M), (Figure 3e, S14c and S14d) showed a linear decrease in T_e proportional with the decrease in the **SS-dithiol** concentration. These observations clearly indicate the heterogeneous nucleation of **SS-diOEt** on **SS-dithiol** nuclei rather than a cooperative alternating copolymerization of a heterodimer. Recently we have shown that SIM imaging is very useful for the visualization of multi-component supramolecular fibers with improved resolution, compared to standard diffraction-limited microscopy imaging.[16] Further SIM imaging could be performed using the inherent emission of monomeric components, which avoids the structural modification of monomers often required to improve the resolution of fluorescence imaging. Thus, visualization of the co-assembled solution using SIM microscopy (upon selective excitation and probing through different emission channels) revealed blocky supramolecular polymers with alternating green and red segments of stacked **SS-diOEt** and **SS-dithiol** monomers, respectively (Figure 3f and S17). Since **SS-dithiol** also gets excited at the **SS-diOEt** excitation (green channel) due to its broad absorption (Figure S7), we observe a continuous green-emitting chain in green channel due to the contribution from both monomers. However, the low photo luminescence emission of **SS-dithiol** (upon excitation in green channel) expected to provide a low green intensity in **SS-dithiol** segment as compared to the highly intense green emission from the **SS-diOEt** blocks. This is exactly observed from the green intensity profile over a micrometer long fiber, which showed a variation in green emission depending on the nature of segments (Figure 3f). Additionally, visualizing through the red channel and corresponding intensity profiles selectively confirmed the presence of red **SS-dithiol** segment. Complementary nature of red

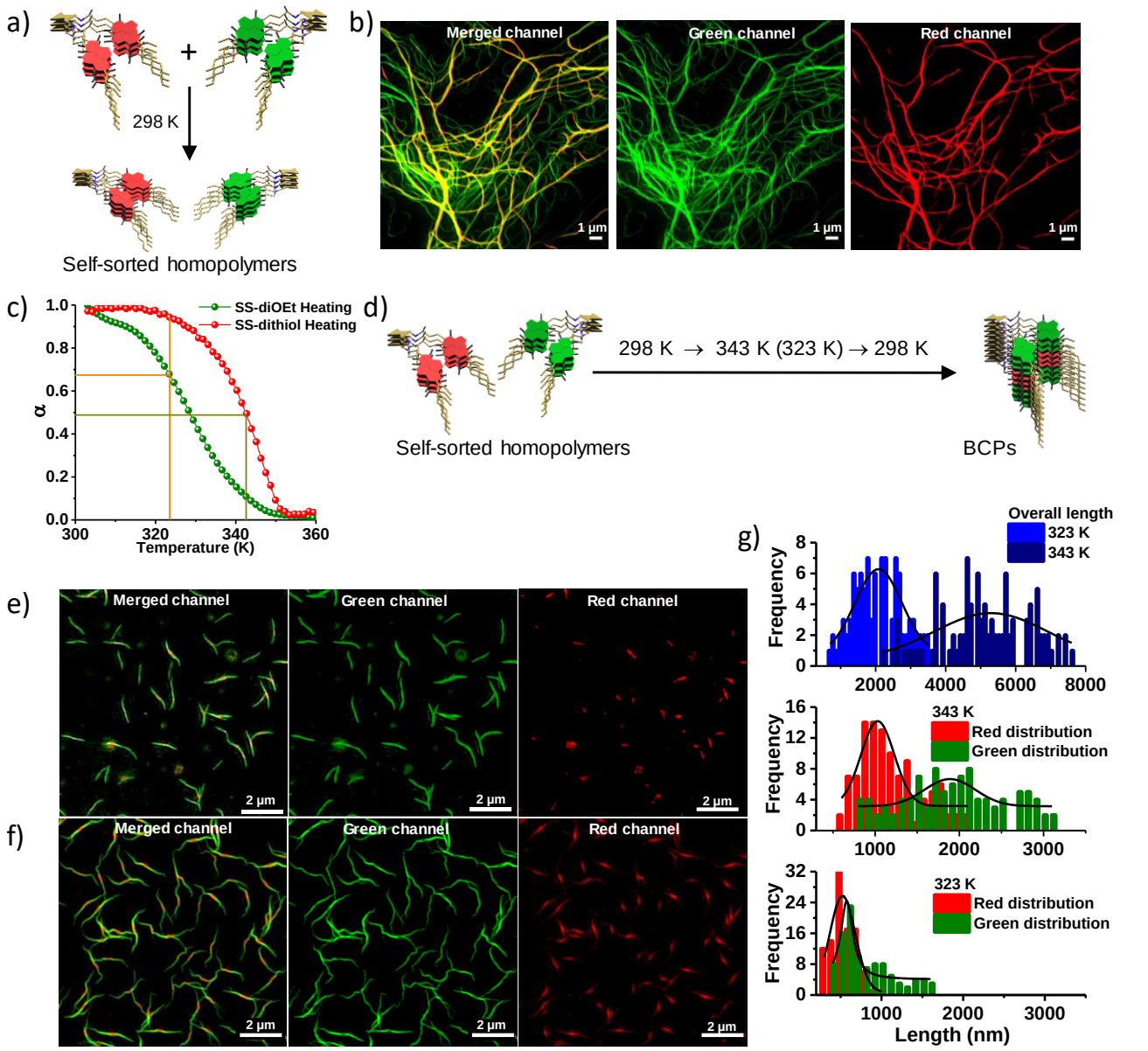

Figure 4. Distribution Analyses of Tri-block Microstructures: (a) Schematic illustration and (b) SIM images of post-synthetically mixed **SS-diOEt** and **SS-dithiol** homopolymers in green, red and merged channels, showing narcissistically self-sorted stacks. (c) Heating curves of the supramolecular homopolymers of **SS-diOEt** and **SS-dithiol** ($c = 2.5\times10^{-5}$ M, 1K/min heating rate) obtained by probing the temperature-dependent absorbance changes at 480 nm for **SS-diOEt** and 550 nm for **SS-dithiol**; which shows higher stability for **SS-dithiol** in comparison to **SS-diOEt** stacks. (d) Schematic illustration of the annealing induced reorganization of self-sorted homopolymers to tri-BCPs by slow cooling form 343 K and 323 K. SIM microscopy images of BCPs in green, red and merged channel obtained via annealing from (e) 323 K and (f) 343 K (heating rate = cooling rate = 1 K/min). (g) Contour length distribution analyses showing the average lengths of the BCPs (above) and both green and red blocks, upon the annealing process from 323 K and 343 K to 298 K. In each case, 100 individual BCP chains were counted to construct the distribution. ([**SS-diOEt**] = [**SS-dithiol**] = 2.5×10^{-5} M, TCE/MCH, 25/75 (v/v), l = 10 mm, (green channel: λ_{ex} = 488 nm, λ_{coll} = 495–575 nm), (red channel: λ_{ex} = 561 nm, λ_{coll} = 570–650 nm)).

and green intensity profiles from the merged channel unequivocally proved the presence of an alternate segmental organization. Blocky organization of the components in the supramolecular copolymer rather than an alternating monomer sequence originates from the lower hetero-free energy gain ($\Delta G_{SS\text{-}diOEt\text{-}SS\text{-}dithiol}$) compared to the total homo-free energy gain ($\Delta G_{SS\text{-}diOEt\text{-}SS\text{-}diOEt}$, $\Delta G_{SS\text{-}dithiol\text{-}SS\text{-}dithiol}$), as reported by Meijer and coworkers (*vide supra*).[16] Melting temperature (T_m) obtained from the heating curve of the supramolecular block copolymer (heating rate = 1 K/min) shows an increase in stability of **SS-diOEt** segment from 322 K to 335 K and a decrease in stability of **SS-dithiol** segment from 341 K to 334 K, compared to the corresponding pure components at similar concentrations (Figure S18 and Table S8). This further rule out any narcissistically self-sorted arrangement between **SS-diOEt** and **SS-dithiol** stacks which would have resulted in similar stability for both individual stacks and the mixture.

Annealing induced modulation of block length distribution

Mixing of the supramolecular homopolymers of **SS-diOEt** and **SS-dithiol** ($c = 2.5\times10^{-5}$ M, TCE/MCH, 25/75 (v/v)) at room temperature results in narcissistically self-sorted green and red chains as evident from SIM microscopic images (Figures 4a, 4b and S20). The self-sorted supramolecular stacks remain intact with time at room temperature, as evident from the spectroscopic and microscopic studies performed after two days, suggesting that these systems are less dynamic at room temperature (Figure S21). This observation is further consistent with the CG MetaD simulations, which revealed a slow monomer exchange dynamics, especially in the **SS-diOEt** stacks, compared to similar stacks reported in the literature,[16] which in this case can be also computed to the monomer conformational transitions associated with the exchange process (Figure 2d). As mentioned earlier, the considerable interaction energy between the monomers of **SS-diOEt** may prevent the monomer from re-shuffling between the two stacks at room temperature. However, heating curves of **SS-diOEt** and **SS-dithiol** supramolecular homopolymers at similar concentrations ($c = 2.5\times10^{-5}$ M) showed differential stability, with higher melting temperature (T_m) for **SS-dithiol** (T_m= 342 K) stacks compared to the assemblies of **SS-diOEt** (T_m = 328 K) (Figure 4c and S22). The lower stability of **SS-diOEt** supramolecular homopolymers seen in the experiments can be attributed to the intrinsically more disordered nature (in terms of the internal organization of the monomers). In fact, a detailed analysis of the internal ordering of these fibers inferred from the MD simulations indicate the presence of defects along the stacks,[30c,31] while these are more present in **SS-diOEt** than in **SS-dithiol** (*vide supra*).

We have annealed the mixture of homopolymers at two temperatures (323 K and 353 K) in an attempt to investigate the effect of monomer exchange dynamics in the reorganization of structure and also to modulate the length distribution of the blocks (Figure 4d). Thus, we sought of increasing the temperature of the system to increase the monomer exchange dynamics (Figure 4c). Further, we anticipated that the difference in the extent of melting of two homopolymers at a higher temperature would lead to differential exchange dynamics for the two segments, and hence cooling down from high temperatures would affect the length distribution of the blocky segments in the resulting supramolecular copolymers. Interestingly on cooling the self-sorted solution of the homopolymers from (heating and cooling rate = 1 K/min) 323 K and 353 K to room temperature leads to the formation of isolated supramolecular BCP chains as evident from the SIM images (Figure 4e and 4f). Large number of isolated chains in the SIM image allowed us to perform an unprecedented statistical analysis on dynamic supramolecular BCPs to extract the degree of polymerization, block lengths, and dispersity similar to studies performed on polymeric blocky cylindrical micelles.[8,9] Figure 4g shows the contour length distributions (CLD) of the degree of polymerization (top panel) and lengths of both block segments (middle and bottom), of the supramolecular BCPs obtained from the analysis of 100 discrete chains from SIM images. CLD analyses showed that the supramolecular BCPs formed by the annealing showed excellent dispersity and length control as evident from the weight average length (L_w), number average length (L_n), and the polydispersity index (PDI). The overall length of the supramolecular BCP chains obtained by annealing from 323K was calculated to be 2090 nm (L_n) and 2322 nm (L_w) with a PDI of 1.11. On the other hand, stacks obtained by annealing from 343 K showed an increase in the degree of polymerization as evident from the increased L_n and L_w of 5075 nm and 5393 nm, respectively with a PDI of 1.06 (Table S10). A similar trend was also observed in the length distribution of both green and red block segments. L_n and L_w values for green blocks (**SS-diOEt)** in the supramolecular block copolymer annealed from 323 K, was calculated to be 800 nm and 935 nm (PDI~ 1.16), whereas the red blocks (**SS-dithiol)** exhibited L_n and L_w values of 540 nm and 581 nm (PDI~1.07), respectively (Figure 4g, Table S11 and S12). However, in supramolecular BCPs from 343 K, the length of both blocks was increased leading to an increase in the overall length of the multi-component stacks (Green: L_n = 1915 nm, L_w = 2115 nm, PDI = 1.10; Red: L_n = 1195 nm, L_w = 1306 nm, PDI = 1.09) (Table S11 and S12).

It is worth noting that both the number and weight average lengths of the green ((**SS-diOEt)** blocks are always higher than that of the red blocks ((**SS-dithiol)** in the supramolecular block copolymers. We envisage that this could be due to the significantly higher interactions between the monomers of SS-**diOEt** compared to that **of SS-dithiol** monomers. This is like the chain copolymerization process of covalent systems, where higher reactivity of one of the monomers leads to the larger block length of that monomer. The length distribution analysis could not be measured for the extended supramolecular blocky copolymers obtained via the cooperative growth from the monomeric state at 363 K (Figure 3) due to the entangled network of green and red segments. Interestingly, the topology of the supramolecular BCP synthesized by annealing the self-sorted homopolymers from 343 K and 323 K are found to be a green-red-green triblock microstructure with a narrow dispersity. This observation is in support of the spectroscopic studies, which showed that nucleation of **SS-dithiol** monomers with higher T_e and subsequent heterogeneous seeded growth of the **SS-diOEt** monomers in a cooperative manner triggers the supramolecular block copolymerization.

Directional energy harvesting in axial organic heterostructures

As there is a considerable amount of overlap between the emission spectrum of **SS-diOEt** (energy donor) and the absorption spectrum of **SS-dithiol** (energy acceptor) monomers organized in the supramolecular block copolymers, we anticipated efficient energy migration along the π-stacked chromophores organized along the fibers. Indeed, the bulk solution phase emission spectrum of these supramolecular donor-acceptor block copolymers, when excited the donor monomers (λ_{ex} = 430 nm), showed a quenching of donor emission (510 nm) with a concomitant two-fold enhancement of the acceptor emission intensity (560 nm) when compared with the direct excitation of the acceptor (λ_{ex} = 530 nm) (Figure S16). Such amplification in acceptor emission along with the quenching of the donor emission indicates the possibility of excitonic migration and energy transfer between the donor-acceptor block segments.[37]

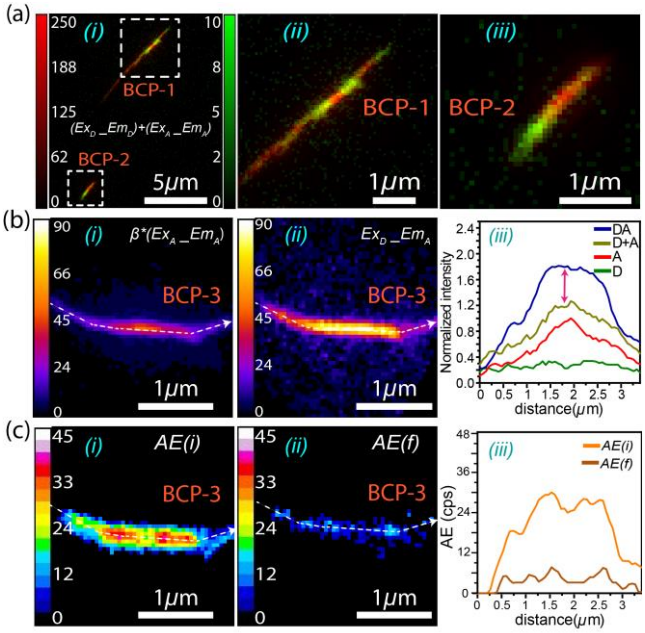

Figure 5. Light-Harvesting Organic Heterostructures: Spatially and spectrally resolved fluorescence images of individual supramolecular block copolymers (BCPs). Pseudo-colour co-localized average photoluminescence (PL) image of BCP heterostructures is in a(i) and corresponding two representative fibrils BCP-1 and BCP-2 are in a(ii) and a(iii). The PL image b(i) is the expected emission of only acceptors (EmA) via direct excitation with 405 nm (ExD), and the sensitized emission of acceptors from the same BCP fibril is b(ii). The corresponding normalized intensity line profiles (along white dashed arrow) (b(iii)), showing the relative A-channel emission (EmA) via 405 nm excitation (ExD) of individual donor and acceptor (D, A), their cumulative intensity (D+A), and sensitized emission due to energy transfer (DA). Intensities are normalized with the acceptor emission intensity. The spatially resolved acceptor intensity enhancement (AE) of BCP-3 at pre- and post-acceptor photo-bleaching are in c(i) and c(ii) respectively, and the corresponding line profiles are in c(iii).

The donors and the acceptors have arranged themselves in a segmented fashion within a single supramolecular BCP, where the acceptor segment resides at the middle and donor towards both ends (Figure 4e and 4f). This topology with alternatively stacked chromophoric segments (with either electronic or optical complementary monomers) of 300-500 nm length can be called as organic axial nano-heterostructures with linear donor-acceptor interface or junctions, reminiscent of well-studied class of inorganic axial heterostructures.[24] This type of segmented arrangement of chromophores encouraged us to look into the energy transfer within a single D-A-D axial heterostructure. We wanted to investigate whether upon the excitation of donor molecules, any directional transfer of energy into the acceptor part occurs or not?

To investigate the possibility of excitation energy migration, we performed spectrally-resolved fluorescence microscopy of individual block copolymerized (BCP) heterostructures. First, we identified single BCP fibrils via direct excitation of the donor and acceptor blocks, with the collection of respective emissions in two energetically separated (D and A) detection channels. Careful superposition of these two images of the same area allowed us to generate an energy-mapped pseudo color co-localized image that provides quantitative information on the spatial variation in the intensity of donors (colored green) and acceptors (colored red). In such energy-mapped color images (Figure 5a(i)), several spatially segregated single BCP fibrils with donor and acceptor blocks can be readily visualized.

Two representative BCP fibrils, BCP-1, and BCP-2 are shown in Figure 5a (ii and iii), which clearly depict the alternating segment distribution of donor and acceptor blocks within each BCP fibril. It is interesting to note that, we always find that the donor segments within the BCP fibrils have extremely feeble fluorescence when excited directly. This is in stark contrast to donor-only fibrils, where the emission is (typically) at least an order of magnitude higher when imaged under identical conditions (Figure S26). This dramatic quenching of emission intensity of donors provides indirect evidence of excitation energy migration from the donor blocks to adjacent acceptor blocks within the BCP fibrils. To thoroughly investigate energy transfer (or excitation energy migration) between donor and acceptor blocks, we performed dual-excitation sensitized emission imaging (see B.1.1. supporting information) of individual BCP heterostructures.[35] This was achieved by imaging of the acceptor emission (545-635 nm) for a single fibril (BCP-3) via separately exciting the acceptors (λ_{ex} = 532 nm) and the donors (λ_{ex} = 405 nm).

First, we obtained a fluorescence intensity image of BCP-3 via direct excitation of the acceptors, which was then factorized by the relative change in the extinction coefficients of the acceptor at the two excitation wavelengths (ε405/ε532). This operation yields the emission intensity of the acceptors due to their direct excitation at the donor excitation wavelength (Figure 5b(i)). As the contribution of the donor emission in the acceptor channel was nominal (verified using pure donor blocks excited at 405 nm, see B.2.1. in supporting information and Figure S25b), Figure 5b(i) effectively portrays the maximum expected emission intensity over the entire BCP fibril in the absence of any energy transfer. However, upon selective excitation of the donors in the single BCP fibrils, we find significantly enhanced emission in the acceptor segment (Figure 5b(ii)), attributed to the sensitized emission of the acceptors (via donors). Such enhancement of the acceptor emission, as portrayed in the spatial distribution of intensities over BCP-3 (Figure 5b(iii)), serves as an unambiguous indicator of excitation energy transfer from flacking donor blocks to adjacent acceptor blocks in each BCP fibril.

The sensitized fluorescence image of BCP-3 (Figure 5c(i)) depicts the acceptor intensity enhancement (AE) due to energy transfer from donors (method **2** supporting information). Interestingly, we find substantial spatial non-uniformity in the AE for a single BCP fibril; for instance, the central region of BCP-3 has considerably lower sensitized emission owing to the absence of the donors within the acceptor segment as compared to that in the interface regions where both donors and acceptors are present. Further, we checked with narcissistically self-sorted donor and acceptor supramolecular stacks and observed AE only at regions where both fibrils are in contact due to the close proximity of donors and

acceptors (Figure S28). To corroborate whether the observed enhancement of acceptor emission (Figure 5c(i)) indeed owes to excitation migration from the donor segments,[36] we selectively photo-bleached the acceptors of BCP-3 using intense 532 nm laser excitation such that the donor molecules remain unaffected. We find that upon progressive irreversible photobleaching of acceptors, there is a concurrent enhancement in the emission of donors (Figure S27), owing to the unavailability of enough acceptors to transfer their excitation energy. Because of the obstruction in this process, the sensitized emission image of BCP-3 after photo-degradation of the acceptors (Figure 5c(ii)) shows nominal AE. It is relevant to mention that spatially-resolved fluorescence spectroscopy measurements on single BCP heterostructures (Figure S29) further validate the **inferences of the** above dual-excitation sensitized emission imaging, and therefore provides direct support to the hypothesis of energy migration between adjacent segments within individual block copolymers .[37]

Conclusion

In conclusion, we have explored the cooperative supramolecular block copolymerization of optically distinct cNDI monomers with slightly different substituents at the core for the synthesis of the light-harvesting organic heterostructure. The characteristic and distinct optical properties of cNDI derivatives, which are sensitive to intermolecular interactions aided the spectroscopic probing of the microstructure during thermodynamically driven supramolecular copolymerization. Distinct green and red fluorescence of the **SS-diOEt** and **SS-dithiol** stacked monomers, respectively facilitated the structural characterization of multi-block microstructure of these supramolecular BCPs via the visualization through SIM-based super resolution imaging. Further, the effective fluorescence imaging allowed a unique size distribution analysis of individual blocks which showed a narrow polydispersity with a PDI of 1.1. The free-energy data for the **SS-dithiol** and **SS-diOEt** intermixing and the comprehension of the exchange mechanisms in these BCPs obtained from the CG simulations helped us in rationalizing the experimental results. A detailed computational study of the exchange mechanism and of defects inside these fibers helped us to rationalize the dynamic behavior of these assemblies and their dynamic tendency/limitation to co-assemble. Finally, spectrally resolved FRET-based microscopy studies on single BCP chains, showed directional light-harvesting along the axial hetero-junctions, thus demonstrating its remarkable potential as functional organic heterostructures.

Supramolecular block copolymerization from the monomeric state of components presented here follows a nucleation-elongation growth mechanism and hence reminiscent of classical chain-growth copolymerization of covalent polymers, where blocky organization of monomers is determined by its reactivity ratio. We envisage that this synthetic strategy can be generalized for the synthesis of a variety of axial organic heterostructures with stable segmented microstructure for diverse optoelectronic applications and catalysis.

ASSOCIATED CONTENT

Supporting Information

Synthetic Schemes, procedures, supporting experimental figures, characterization spectra, extended computational methods and procedures. This material is available free of charge via the Internet at http://pubs.acs.org."

AUTHOR INFORMATION

*Corresponding Author

*george@jncasr.ac.in

*arindam@chem.iitb.ac.in

*giovanni.pavan@polito.it

*sagasti@jncasr.ac.in

Author Contributions

The manuscript was written through contribution of all authors. All authors have given approval to the final version of the manuscript

ACKNOWLEDGMENT

We thank Prof. C. N. R. Rao, FRS for his support and guidance. We would also like to thank JNCASR and the Department of Science and Technology, Government of India, for financial support. S. J. G. acknowledges the funding received from Department of Biotechnology, Government of India for the Indo-Switzerland Joint Research project (BT/IN/Swiss/55/SJG/2018-2019). A.S., R.S. and T.B. thanks CSIR for fellowship. G. M. P. acknowledges the funding received by the Swiss National Science Foundation (SNSF grants IZLIZ2_183336) and by the European Research Council (ERC) under the European Union's Horizon 2020 research and innovation programme (grant agreement no. 818776 - DYNAPOL).

ABBREVIATIONS

AE, acceptor intensity enhancement.

REFERENCES

(1) (a) De Greef, T. F. A.; Smulders, M. M. J.; Wolffs, M.; Schenning, A. P. H. J.; Sijbesma, R. P.; Meijer, E. W. Supramolecular polymerization. *Chem. Rev.* **2009**, *109*, 5687–5754. (b) de Greef, T. F. A.; Meijer, E. W. Supramolecular polymers. *Nature* **2008**, *453*, 171-173. (c) Aida, T.; Meijer, E. W.; Stupp, S. I. Functional Supramolecular Polymers. *Science* **2012**, *335*, 813-817. (d) Vantomme, G.; Meijer, E. W. The construction of supramolecular systems. *Science* **2019**, *363*, 1396-1397. (e) Aida, T. On Supramolecular Polymerization: Interview with Takuzo Aida. *Adv. Mater.* **2019**, 1905445. (f) Aida, T.; Meijer, E. W. Supramolecular Polymers – we've Come Full Circle. *Isr. J. Chem.* **2020**, *60*, 33–47.

(2) (a) Adelizzi, B.; Van Zee, N. J.; De Windt, L. N.; Palmans, A. R.; Meijer, E. W. Future of supramolecular copolymers unveiled by reflecting on covalent copolymerization. *J. Am. Chem. Soc.* **2019**, *141*, 6110-6121. (b) Wehner, M.; Würthner, F. Supramolecular polymerization through kinetic pathway control and living chain growth. *Nat. Rev. Chem.* **2020**, *4*, 38-53. (c) Besenius, Pol. Controlling supramolecular polymerization through multicomponent self-assembly. *Polymer Chemistry* **2017**, 55, 34–78.

(3) (a) Jain, A.; George, S. J. New directions in supramolecular electronics. *Mater. Today* **2015**, *18*, 206-214. (b) Jain, A.; George, S. J. Meshing organic nanowires. *Nat. Nanotech.* **2016**, *11*, 843-844.

(4) (a) Lutz, J. F.; Ouchi, M.; Liu, D. R.; Sawamoto, M. Sequence controlled polymers. *Science* **2013**, *341*, 1238149. (b) Schacher, F. H.; Rupar, P. A.; Manners, I. Functional block copolymers: nanostructured materials with emerging applications. *Angew. Chem., Int. Ed.* **2012**, *51*, 7898–7921.

(5) (a) Frisch, H.; Unsleber, J. P.; Lgdeker, D.; Peterlechner, M.; Brunklaus, G.; Waller, M.; Besenius, P. pH-Switchable ampholytic supramolecular copolymers. *Angew. Chem., Int. Ed.* **2013**, 52, 10097–10101. (b) Frisch, H.; Fritz, E.; Stricker, F.; Schmüser, L.; Spitzer, D.; Weidner, T.; Ravoo, B. J.; Besenius, P. Kinetically con-trolled sequential growth of surface-grafted chiral supramolecular copolymers. *Angew. Chem., Int. Ed.* **2016**, 55, 7242 – 7246. (c) Zhang, X.; Wang, C. Supramolecular amphiphiles. *Chem. Soc. Rev.* **2011**, *40*, 94-101. (d) Wang, C.; Guo, Y.; Wang, Y.; Xu, H.; Wang, R.; Zhang, X. Supramolecular amphiphiles based on a water-soluble charge-transfer complex: fabrication of ultralong nanofibers with tunable straightness. *Angew. Chem., Int. Ed.* **2009**, *48*, 8962–896. (e) Appel, E. A.; Biedermann, F.; Rauwald, U.; Jones, S. T.; Zayed, J. M.; Scherman, O. A. Supramolecular cross-linked networks via host guest complexation with cucurbit[8]uril. *J. Am. Chem. Soc.* **2010**, *132*, 14251-14260.

(6) (a) Van Gestel, J.; Palmans, A. R. A.; Titulaer, B.; Vekemans, J. A. J. M.; Meijer, E. W. "Majority-Rules" operative in Chiral Columnar Stacks of C3-Symmetrical Molecules. *J. Am. Chem. Soc.* **2005**, *127*, 5490–5494. (b) Smulders, M. M. J.; Schenning, A. P. H. J.; Meijer, E. W. Insight into the Mechanisms of Cooperative Self-Assembly: The "Sergeants-and-Soldiers" Principle of Chiral and Achiral C3-Symmetrical Discotic Triamides. *J. Am. Chem. Soc.* **2008**, *130*, 606–611. (c) Jin, W.; Fukushima, T.; Niki, M.; Kosaka, A.; Ishii, N.; Aida, T. Self-Assembled Graphitic Nanotubes with One-Handed Helical Arrays of a Chiral Amphiphilic Molecular Graphene. *Proc. Natl. Acad. Sci.* **2005**, *102*, 10801–10806. (d) Helmich, F.; Smulders, M. M. J.; Lee, C. C.; Schenning, A. P. H. J.; Meijer, E. W. Effect of Stereogenic Centers on the Self-Sorting, Depolymerization, and Atropisomerization Kinetics of Porphyrin-Based Aggregates. *J. Am. Chem. Soc.* **2011**, *133*, 12238–12246. (e) Kim, T.; Mori, T.; Aida, T.; Miyajima, D. Dynamic Propeller Conformation for the Unprecedentedly High Degree of Chiral Amplification of Supramolecular Helices. *Chem. Sci.* **2016**, *7*, 6689–6694. (f) Ajayaghosh, A.; Varghese, R.; George, S. J.; Vijayakumar, C. Transcription and Amplification of Molecular Chirality to Oppositely Biased Supramolecular π Helices. *Angew. Chem., Int. Ed.* **2006**, *45*, 1141–1144. (g) García, F.; Sánchez, L. Structural Rules for the Chiral Supramolecular Organization of OPEbased Discotics: Induction of Helicity and Amplification of Chirality. *J. Am. Chem. Soc.* **2012**, *134*, 734–742. (h) Smulders, M. M. J.; Stals, P. J. M.; Mes, T.; Paffen, T. F. E.; Schenning, A. P. H. J.; Palmans, A. R. A.; Meijer, E. W. Probing the Limits of the Majority-Rules Principle in a Dynamic Supramolecular Polymer. *J. Am. Chem. Soc.* **2010**, *132*, 620–626. (i) Coelho, J. P.; Matern, J.; Albuquerque, R. Q.; Fernández, G. Mechanistic Insights into Statistical Co-Assembly of Metal Complexes. *Chem. Eur. J.* **2019**, *25*, 8960-8964.

(7) (a) Yagai, S.; Hamamura, S.; Wang, H.; Stepanenko, V.; Seki, T.; Unoike, K.; Kikkawa, Y.; Karatsu, T.; Kitamura, A.; Würthner, F. Unconventional Hydrogen-Bond-Directed Hierarchical Co-Assembly between Perylene Bisimide and Azobenzene-Functionalized Melamine. *Org. Biomol. Chem.* **2009**, *7*, 3926–3929. (b) Görl, D.; Zhang, X.; Stepanenko, V.; Würthner, F. Supramolecular Block Copolymers by Kinetically Controlled Co-Self-Assembly of Planar and Core-Twisted Perylene Bisimides. *Nat. Commun.* **2015**, *6*, 7009.

(8) (a) Wang, X.; Guerin, G.; Wang, H.; Wang, Y.; Manners, I.; Winnik, M. Cylindrical block copolymer micelles and co-micelles of controlled length and architecture. *Science* **2007**, *317*, 644–648. (b) Gilroy, J. B.; Gädt, T.; Whittell, G. R.; Chabanne, L.; Mitchels, J. M.; Richardson, R. M.; Winnik, M. A.; Manners, I. Monodisperse cylindrical micelles by crystallization-driven living self-assembly. *Nat. Chem.* **2010**, *2*, 566–570. (c) Hailes, R. L. N.; Oliver, A. M.; Gwyther, J.; Whittell, G. R.; Manners, I. Polyferrocenylsilanes: synthesis, properties, and applications. *Chem. Soc. Rev.*, **2016**, *45*, 5358.

(9) (a) Gädt, T.; Ieong, N. S.; Cambridge, G.; Winnik, M. A.; Manners, I. Complex and hierarchical micelle architectures from diblock copolymers using living, crystallization-driven polymerizations. *Nat. Mater.* **2009**, *8*, 144. (b) Hudson, Z. M.; Boott, C. E.; Robinson, M. E.; Rupar, P. A.; Winnik, M. A.; Manners, I. Tailored hierarchical micelle architectures using living crystallization-driven self-assembly in two dimensions. *Nat. Chem.* **2014**, *6*, 893; (c) He, X.; Hsiao, M.-S.; Boott, C. E.; Harniman, R. L.; Nazemi, A.; Li, X.; Winnik, M. A.; Manners, I. Two-dimensional assemblies from crystallizable homopolymers with charged termini. *Nat. Mater.* **2017**, *16*, 481. (d) Qiu, H.; Gao, Y.; Boott, C. E.; Gould, O. E. C.; Harniman, R. L.; Miles, M. J.; Webb, S. E. D.; Winnik, M. A.; Manners, I. Uniform patchy and hollow rectangular platelet micelles from crystallizable polymer blends. *Science* **2016**, *352*, 697. (e) J. R. Finnegan, D. J. Lunn, O. E. C. Gould, Z. M. Hudson, G. R. Whittell, M. A. Winnik, I. Manners, Gradient crystallization-driven self-assembly: cylindrical micelles with "patchy" segmented coronas via the coassembly of linear and brush block copolymers. *J. Am. Chem. Soc.* **2014**, *136*, 13835-13844. (f) Qiu, H.; Gao, Y.; An Du, V.; Harniman, R.; Winnik, M. A.; Manners, I. Branched micelles by living crystallization-driven block copolymer self-assembly under kinetic control. *J. Am. Chem. Soc.* **2015**, *137*, 2375–2385. (g) Nazemi, A.; He, X.; MacFarlane, L. R.; Harniman, R. L.; Hsiao, M.-S.; Winnik, M. A.; Faul, C. F. J.; Manners, I. Uniform "Patchy" Platelets by Seeded Heteroepitaxial Growth of Crystallizable Polymer Blends in Two Dimensions. *J. Am. Chem. Soc.* **2017**, *139*, 4409-4417.

(10) (a) Zhang, W.; Jin, W.; Fukushima, T.; Saeki, A.; Seki, S.; Aida, T. Supramolecular linear heterojunction composed of graphite-like semiconducting nanotubular segments. *Science* **2011**, *334*, 340–343. (b) Zhang, W.; Jin, W.; Fukushima, T.; Mori, T.; Aida, T. Helix sense-selective supramolecular polymerization seeded by a onehanded helical polymeric assembly. *J. Am. Chem. Soc.* **2015**, *137*, 13792–13795.

(11) Jung, S.H.; Bochicchio, D.; Pavan, G.M.; Takeuchi, M.; Sugiyasu, K. A block supramolecular polymer and its kinetically enhanced stability. *J. Am. Chem. Soc.* **2018**, *140*, 10570-10577.

(12) (a) Fukui, T.; Kawai, S.; Fujinuma, S.; Matsushita, Y.; Yasuda, T.; Sakurai, T.; Seki, S.; Takeuchi, M.; Sugiyasu, K. Control over differentiation of a metastable supramolecular assembly in one and two dimensions. *Nat. Chem.* **2017**, *9*, 493-499. (b) Ogi, S.; Sugiyasu, K.; Manna, S.; Samitsu, S.; Takeuchi, M. Living supramolecular polymerization realized through a biomimetic approach. *Nat. Chem.* **2014**, *6*, 188-195. (c) Ogi, S.; Stepanenko, V.; Sugiyasu, K.; Takeuchi, M.; Würthner, F. Mechanism of self-assem-bly process and seeded supramolecular polymerization of perylene bisimide organogelator. *J. Am. Chem. Soc.* **2015**, *137*, 3300-3307. (d) Dhiman, S.; George, S. J. Temporally controlled supramolecular polymerization. *Bull. Chem. Soc. Jpn.* **2018**, *91*, 687– 699. (e) Matern, J.; Dorca, Y.; Sánchez, L.; Fernández, G. Revising complex supra-molecular polymerization under kinetic and thermodynamic control. *Angew. Chem., Int. Ed.* **2019**, *58*, 16730-16740. (f) van der Zwaag, D.; De Greef, T. F. A.; Meijer, E. W. Programmable supramolecular polymerizations. *Angew. Chem., Int. Ed.* **2015**, *54*, 8334–8336. (g) Mukhopadhyay, R. D.; Ajayaghosh, A. Living supramolecular polymerization. *Science* **2015**, *349*, 241. (h) Würthner, F. Living it up. *Nat. Chem.* **2014**, *6*, 171-173.

(13) (a) Mishra, A.; Korlepara, D. B.; Kumar, M.; Jain, A.; Jonnalagadda, N.; Bejagam, K. K.; Balasubramanian, S.; George, S. J. Biomimetic temporal self-assembly via fuel-driven controlled supramolecular polymerization. *Nat. Commun.* **2018**, *9*, 1295. (b) Jain, A.; Dhiman, S.; Dhayani, A.; Vemula, P. K.; George, S. J. Chemical fuel-driven living and transient supramolecular polymerization. *Nat. Commun.* **2019**, *10*, 450. (c) Ogi, S.; Stepanenko, V.; Thein, J.; Würthner, F. Impact of alkyl spacer length on aggregation pathways in kinetically controlled supramolecular polymerization. *J. Am. Chem. Soc.* **2016**, *138*, 670-678. (d) Ogi, S.; Matsumoto, K.; Yamaguchi, S. Seeded polymerization through the interplay of folding and aggregation of an amino-acid-based diamide. *Angew. Chem., Int. Ed.* **2018**, 57, 2339–2343. (e) Greciano, E. E.; Matarranz, B.; Sánchez, L. Pathway complexity versus hierarchical self-assembly in N-annulated perylenes: Structural effects in seeded supramo-lecular polymerization. *Angew. Chem., Int. Ed.* **2018**, 57, 4697–4701. (f) Endo, M.; Fukui, T.; Jung, S. H.; Yagai, S.; Takeuchi, M.; Sugiyasu, K. Photoregulated living supramolecular polymerization established by combining energy landscapes of photoisomerization and nucleation–elongation processes. *J. Am. Chem. Soc.* **2016**, *138*, 14347–14353. (g) Langenstroer, A.; Kartha, K. K.; Dorca, Y.; Droste, J.; Stepanenko, V.; Albuquerque, R. Q.; Hansen, M. R.; Sánchez, L.;

Fernández G. Unraveling concomitant packing polymorphism in metallosupramolecular polymers. *J. Am. Chem. Soc.* **2019**, *141*, 5192–5200. (h) Wilkins, C. J.; He, X.; Symons, H. E.; Harniman, R. L.; Faul, C. F. J.; Manners, I. Living supramolecular polymerisation of perylene diimide amphiphiles by seeded growth under kinetic control. *Chem. Eur. J.* **2018**, *24*, 15556-15565. (i) Robinson, M. E.; Lunn, D. J.; Nazemi, A.; Whittell, G. R.; De Cola, L.; Manners, I. Length control of supramolecular polymeric nanofibers based on stacked planar platinum(ii) complexes by seeded-growth. *Chem. Commun.* **2015**, *51*, 3715921 –15924. (j) Aliprandi, A.; Mauro, M.; Cola, L. D. Controlling and imaging biomimetic self-assembly. *Nat. Chem.* **2016**, *8*, 10-15. (k) Kemper, B.; Zengerling, L.; Spitzer, D.; Otter, R.; Bauer, T.; Besenius, P. Kinetically controlled stepwise self-assembly of AuI-metallopeptides in water. *J. Am. Chem. Soc.* **2018**, *140*, 534-537.

(14) (a) Wagner, W.; Wehner, M.; Stepanenko, V.; Würthner, F. Supramolecular block copolymers by seeded living polymerization of perylene bisimides. *J. Am. Chem. Soc.* **2019**, *141*, 12044-12054. (b) Wagner, W.; Wehner, M.; Stepanenko, V.; Würthner, F. *CCS Chem.* **2019**, *1*, 598–613.

(15) (a) Sakai, N.; Mareda, J.; Vauthey, E.; Matile, S. Core-substituted Naphthalenediimides. *Chem., Commun.* **2010**, *46*, 4225-4237. (b) Sarkar, A.; Kölsch, J. C.; Berač, C. M.; Venugopal, A.; Sasmal, R.; Otter, R.; Besenius, P.; Georg, S. J. *ChemistryOpen* **2020**, *9*, 346–350.

(16) Sarkar, A.; Sasmal, R.; Empereur-mot, C.; Bochicchio, D.; Kompella, S. V. K.; Sharma, K.; Dhiman, S.; Sundaram, B.; Agasti, S. S.; Pavan, G. M.; George, S. J. Self-Sorted, Random, and Block Supramolecular Copolymers via Sequence Controlled, Multicomponent Self-Assembly. *J. Am. Chem. Soc.* **2020**, doi.org/10.1021/jacs.0c01822.

(17) (a) Lutz, J. F.; Lehn, J-M.; Meijer, E. W.; Matyjaszewski, K. From precision polymers to complex materials and systems. *Nat. Rev. Mater.* **2016**, *1*, 16024-16038. (b) Szwarc, M.; Nature 1956, *178*, 1168–1169. (c) Matyjaszewski, K.; Xia, J. *Chem. Rev.* **2001**, *101*, 2921-2990.

(18) Odian, G. G. Principle of Polymerization, Third Ed.; Wiley, Ed.; 1991.

(19) (a) Kulkarni, C.; Balasubramanian, S.; George, S. J. What molecular features govern the mechanism of supramolecular polymerization? *ChemPhysChem* **2013**, *14*, 661 – 673. (b) Jonkheijm, P.; van der Schoot, P.; Schenning, A. P. H. J.; Meijer, E. W. Probing the solvent-assisted nucleation pathway in chemical self-assembly. *Science* **2006**, *313*, 80-83. (c) Kulkarni, C.; Bejagam, K. K.; Senanayak, P. S.; Narayan, K. S.; Balasubramanian, S.; George, S. J. Dipole-moment-driven cooperative supramolecular polymerization. *J. Am. Chem. Soc.* **2015**, *137*, 3924-3932.

(20) Kitamoto, Y.; Pan, Z.; Prabhu, D. D.; Isobe, A.; Ohba, T.; Shimizu, N.; Takagi, H.; Haruki, R.; Adachi, S. I.; Yagai, S. One-shot preparation of topologically chimeric nanofibers via a gradient supramolecular copolymerization. *Nat. Commun.* **2019**, *10*, 4578.

(21) Adelizzi, B.; Aloi, A.; Markvoort, A. J.; Ten Eikelder, H. M.; Voets, I. K.; Palmans, A. R.; Meijer, E. W. Supramolecular block copolymers under thermodynamic control. *J. Am. Chem. Soc.* **2018**, *140*, 7168-7175.

(22) Adelizzi, B.; Aloi, A.; Van Zee, N. J.; Palmans, A. R. A.; Meijer, 939E. W.; Voets, I. K. Painting Supramolecular Polymers in Organic Solvents by Super-resolution Microscopy. *ACS Nano* **2018**, *12*, 4431–9414439. (b) Kubota, R.; Nakamura, K.; Torigoe, S.; Hamachi, I. The Power of Confocal Laser Scanning Microscopy in Supramolecular Chem-istry: In situ real-time imaging of stimuli-responsive multicompo-nent supramolecular hydrogels. *ChemistryOpen* **2020**, *9*, 67–79. (c) Albertazzi, L.; Zwaag, D. v. d.; Leenders, C. M. A.; Fitzner, R.; van der Hofstad, R. W.; Meijer, E. W. Probing Exchange Pathways in One-Dimensional Aggregates with Super-Resolution Microscopy. *Science* **2014**, *344*, 491-495.

(23) Schenning, A. P. H. J.; Meijer, E. W. Supramolecular electronics; nanowires from self-assembled π-conjugated systems. *Chem. Commun.* **2005**, *26*, 3245–3258.

(24) (a) Yang, C.; Barrelet, C.J.; Capasso, F.; Lieber, C. M. Single p-Type/Intrinsic/n-Type Silicon Nanowires as Nanoscale Avalanche Photodetectors. *Nano Letters* **2006**, *6*, 2929-2934. (b) Tian, B.; Zheng, X.; Kempa, T. J.; Fang, Y.; Yu, N.; Yu, G.; Huang, J.; Lieber, C.M. Coaxial silicon nanowires as solar cells and nanoelec-tronic power sources. *Nature*, **2007**, *449*, 885-889. (c) Costi R.; Saunders E. A.; Elmalem E.; Salant A.; Banin, U. Visible Light-Induced Charge Retention and Photocatalysis with Hybrid CdSe–Au Nanodumbbells. *Nano Letters* **2008**, *8*, 637-641.

(25) Jin, X.; Price, M. B. Finnegan, J. R.; Boott, C. E.; Richter, J. M.; Rao, A.; Menke, S. M.; Friend, R. H.; Whittell, G. R.; Manners, I. Long-range exciton transport in conjugated polymer nanofibers prepared byseeded growth. *Science* **2018**, *360*, 897-900.

(26) Hudson, Z. M.; Lunn, D. J.; Winnik, M. A.; Manners, I. *Nat. Commun.* **2014**, *5*, 3372.

(27) (a) Narayan, B.; Bejagam, K. K.; Balasubramanian, S.; George, S. J. Autoresolution of segregated and mixed p-n stacks by stereoselective supramolecular polymerization in solution. *Angew. Chem., Int. Ed.* **2015**, *54*, 13245–13249. (b) Sarkar, A.; Dhiman, S.; Chalishazar, A.; George, S. J. Visualization of stereoselective supramolecular polymers by chirality-controlled energy transfer. *Angew. Chem., Int. Ed.* **2017**, *56*, 13767 –13771.

(28) (a) ten Eikelder, H. M. M.; Markvoort, A. J.; de Greef, T. F. A.; Hilbers, P. A. J. *J. Phys. Chem. B* **2012**, *116*, 5291. (b) Zhao, D.; Moore, J. S. Nucleation–elongation: a mechanism for cooperative supramolecular polymerization. *Org. Biomol. Chem.* **2003**, *1*, 3471-3491.

(29) (a) Oosawa, F.; Asakura, S. *Academic Press Inc., New York*, **1975**.

(30) (a) Bochicchio, D.; Pavan. G. M. Molecular modelling of supramolecular polymers. *Adv. Phys. X* **2018**, *3*, 1436408. (b) Bochicchio, D.; Pavan. G. M. From Cooperative Self-Assembly to Water-Soluble Supramolecular Polymers Using Coarse-Grained Simulations. *ACS Nano* **2017**, *11*, 1000-1011. (c) Gasparotto, P.; Bochicchio, D.; Ceriotti, M.; Pavan, G. M. Identifying and Tracking Defects in Dynamic Supramolecular Polymers. *J. Phys. Chem. B* **2020**, *124*, 589-599.

(31) Bochicchio, D.; Salvalaglio, M.; Pavan, G. M. Into the Dynamics of a Supramolecular Polymer at Submolecular Resolution. *Nat. commun.* **2017**, *8*, 1-11.

(32) Marrink, S. J.; Risselada, H. J.; Yefimov, S.; Tieleman, D. P.; De Vries, A. H. The MARTINI Force Field: Coarse Grained Model for Biomolecular Simulations. *J. Phys. Chem. B*, **2007**, *111*, 7812-7824.

(33) Barducci, A.; Bussi, G.; Parrinello, M. Well-tempered metadynamics: a smoothly converging and tunable free-energy method. *Physical review letters*, **2008**, *100*, 020603.

(34) Bochicchio, D.; Kwangmettatam, S.; Kudernac, T.; Pavan. G. M. How Defects Control the Out-of-Equilibrium Dissipative Evolution of a Supramolecular Tubule. *ACS Nano* **2019**, *13*, 4322-4334

(35) Das, S.; Sharma, D. K.; Chakrabarty, S.; Chowdhury, A.; Sen Gupta, S. Bioactive Polymersomes Self-Assembled from Amphiphilic PPO-GlycoPolypeptides: Synthesis, Characterization, and Dual-Dye Encapsulation. *Langmuir* **2015**, *31*, 3402–3412.

(36) Berney, C.; Danuser, G. FRET or No FRET: A Quantitative Comparison. *Biophys J.* **2003**, **84**, 3992-4010

(37) (a) Haedler, A. T.; Kreger, K.; Issac, A.; Wittmann, B.; Kivala, M.; Hammer, N.; Köhler, J.; Schmidt, H.-W.; Hildner, R. Long-range energy transport in single supramolecular nanofibres at room temperature. *Nature* **2015**, *9*, 196-200. (b) Wan, Y.; Stradomska, A.; Knoester, J.; Huang, L. Direct Imaging of Exciton Transport in Tubular Porphyrin Aggregates by Ultrafast Microscopy. *J. Am. Chem. Soc.* **2017**, *139*, 21, 7287-7293. (c) Brixner, T.; Hildner, R.; Köhler, J.; Lambert, C.; Würthner, F. Exciton Transport in Molecular Aggregates – From Natural Antennas to Synthetic Chromophore Systems. *Adv. Energy Mater.* **2017**, 1700236.

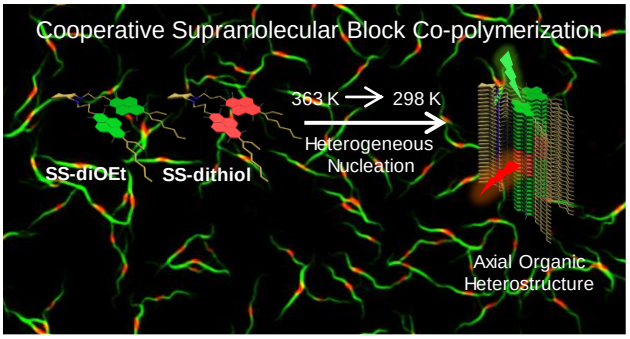

Table of Contents artwork